Directivity Enhancement and Spurious Radiation Suppression in Leaky-Wave Antennas Using Inductive Grid Metasurfaces

Blanco, Darwin; Rajo-Iglesias, Eva; Maci, Stefano; Llombart, Nuria

DOI
10.1109/TAP.2014.2387422

Publication date
2015

Document Version
Accepted author manuscript

Published in
IEEE Transactions on Antennas and Propagation

Directivity Enhancement and Spurious Radiation Suppression in Leaky-Wave Antennas Using Inductive Grid Metasurfaces

Darwin Blanco, Eva Rajo-Iglesias, *Senior Member, IEEE*, Stefano Maci, *Fellow, IEEE*, and Nuria Llombart, *Senior Member, IEEE*

***Abstract*—Fabry-Perot antennas (FPA) achieve high broadside directivity due to the simultaneous excitation of a pair of nearly degenerate TE/TM leaky-wave modes using a partially-reflecting surface on top of a ground plane. This partially-reflecting surface can be obtained using a dielectric superstrate or via a capacitive or inductive metasurface (MTS). By using an equivalence between the conventional dielectric superstrate and the MTS-based structures in terms of the dominant TE/TM modes, we show that the use of inductive grid MTSs leads to a directivity enhancement. A higher roll-of in the radiation patterns is achieved as a result of the intrinsic suppression of the spurious TM_0 leaky wave mode. This suppression is mathematically demonstrated and validated with full-wave simulations. The achieved improvement in more than 1 dB for inductive strip grid based MTS with respect to dielectric based super-layers, for the same frequency band of 2.5%, is verified with measurements. Two prototypes, with the dielectric superlayer and inductive strip grid based MTS, have been fabricated and measured supporting the claim of this work.**

***Index Terms*—Gain enhancement, leaky-wave antennas, metasurfaces, TM_0 mode suppression.**

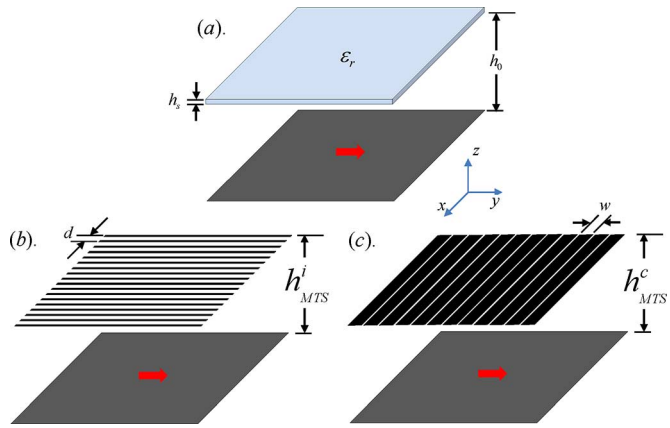

Fig. 1. LW waveguide antenna using (a). a dielectric superstrate with permittivity ϵ_r, (b). an inductive strip grid based MTS and (c). a capacitive slot grid based MTS. The periodicity of the MTS is d, whereas w indicates the strip width. We refer to capacitive MTS when the strips are aligned to the H-plane and to inductive MTS when the strips are aligned to the E-plane.

I. Introduction

THE use of partially reflecting surfaces on top of a ground plane to enhance the directivity of small antennas has been considerably studied in literature [1]–[11]. This type of antennas are typically referred as leaky wave antennas (LWAs) [2]–[5], electromagnetic band-gap (EBG) antennas [7], Fabry-Perot antennas (FPA) [8] and even resonant cavity antennas [11]. Hereinafter, we will refer to these antennas as LWAs. LWAs make use of a partially transmissive resonant structure [2] which can be made of a thin dielectric superstrate [2], [9], [10] or by using inductive- or capacitive-metasurfaces (MTS) [4]–[8], [10]–[14]. Fig. 1 shows three examples of these topologies placed on top of a waveguide opening. Recently, LWAs have gained interest for future Ka-band telecommunication satellites due to their potential to create overlapping radiating areas in focal plane arrays with a single feed per beam [15], [16]. Telecommunication space industries are currently interested in developing future thinned arrays with limited scanning ranges for the Ku-band. Besides other possible approaches based on sub-arrays, there is the interest to investigate the potential of LWAs for this application since they would lead to directive array elements even if the array periodicity is large [17]. In [18], a theoretical study demonstrated the potential of using LW based thinned arrays showing an improved scanning performance with respect to thinned arrays based on free space directive horns. In this study, a direct relationship with the mutual coupling level (directly related to the dielectric constant of the LWA superlayer [19]) and the optimal thinned array spacing was presented. Future telecommunication thinned arrays will operate with spacing of $2\lambda_0$ and a relative frequency bandwidth of 1.7% at Ku-band (14.25–14.5 GHz) with a maximum scanning angle of 8.6^0. This scenario, following the study in [18], would require a dielectric superlayer with $\epsilon_r = 10$. In this work, we investigate which partially reflecting surface, dielectric superstrate or MTS is the most appropriate for this scenario.

The physical phenomenon exploited, in this type of antennas, to achieve high directivity from a point source is the excitation

Manuscript received June 12, 2014; revised November 05, 2014; accepted December 11, 2014. Date of publication January 05, 2015; date of current version March 02, 2015. This work was supported in part by the Spanish Government under project TEC2013-44019-R.

D. Blanco and E. Rajo-Iglesias is with the Dept. of Communications and Signal Theory, Carlos III University, 28911 Madrid, Spain (e-mail: djblanco@tsc.uc3m.es; eva@tsc.uc3m.es).

Stefano Maci is with the Dept. of Information Engineering, University of Siena, Siena 53100, Italy (e-mail: macis@dii.inisi.it).

N. Llombart is with the THz Sensing Group, Delft University of Technology, Delft, The Netherlands (e-mail: n.llombartjuan@tudelft.nl).

Color versions of one or more of the figures in this paper are available online at http://ieeexplore.ieee.org.

of a pair of nearly degenerated $\mathrm{TE}_1/\mathrm{TM}_1$ leaky wave modes. These modes propagate in the resonant region by means of subcritical multiple reflections between the ground plane and the superstrate/MTS, while partially leaking energy in free space. The amount of energy radiated at each reflection is related to the LW attenuation constant and can be controlled by the MTS sheet-impedance or the dielectric constant. For a detuned structure at frequency above the resonant frequency, the far-field radiation pattern exhibits conical shape which eventually degenerates in a pencil beam at the frequency where the real part and imaginary part of the complex leaky wave wavenumber are equal. This occurs almost at the same frequency for both a TE_1 and a TM_1 mode. For the dielectric superlayer, the maximum directivity at broadside is achieved at the resonant condition, i.e., the thickness of the resonant cavity is $h_0 = \lambda_0/2$, and that of the superlayer is $h_s = \lambda_0/4\sqrt{\epsilon_r}$, [2]. Under this condition, the couple of TE/TM leaky wave modes can propagate with same phase velocity, creating a nearly uniform phase distribution in the aperture. It has been seen that the generated aperture field is also very well polarized, due to a compensation effect between the TE and TM modal tangential field components [20]. However, this type of LWA also generates an undesired spurious TM_0 leaky-wave mode, conceptually associated with the TEM mode of the perfectly conducting walls parallel plate waveguide [19]. This mode radiates near the Brewster angle creating spurious lobes in the E-plane reducing the beam efficiency. In this paper, we show that inductive strip grid based MTS leads to higher directivity enhancement in equivalent LWAs by virtue of the suppression of this TM_0 leaky wave mode while maintaining the same frequency bandwidth. In an inductive strip grid based MTS, this TM_0 leaky wave mode is transformed into a surface wave (SW), whereas the capacitive slot grid based MTS and dielectric superstrate do support the leaky wave mode. The effect of this mode can be attenuated by using a double slot feed [19], [21]. Even when this slot feed is used, the strip grid based MTS leads to the highest directivity for the same frequency bandwidth. Other type of MTSs, such as artificial dielectrics made of patches [22], do not alter the TM_0 mode of the hosting stratification, however they lead to lower directivity enhancement because they introduce asymmetries in the propagation constants of the main TE/TM modes [23].

For array applications, it is important to maximize the directivity of the LWA at the largest possible bandwidth and keeping the mutual coupling levels in the order of -20 dB, both (directivity and mutual coupling), are proportional to the $\mathrm{TE}_1/\mathrm{TM}_1$ mode wavenumber [19], [24]. In this paper, we investigate three LWA based on dielectric superstrate, inductive strip grid based MTS, and capacitive slot grid MTS with comparable same $\mathrm{TE}_1/\mathrm{TM}_1$ mode wavenumbers that match the specifications required for future telecommunication thinned arrays. We demonstrated both by full wave simulations and prototype measurements that inductive strip grid based MTS leads to higher directivities than the other two structures.

II. On the Equivalence Between LWAs

In this section, a theoretical comparison with the three types of LWA shown in Fig. 1 is presented. For this purpose, we will investigate how the PRS structures alter the radiation from an elementary magnetic source on an infinite ground plane. A dielectric superlayer or MTS will be located on top of the ground plane at a certain height, h_0 or $\mathrm{h}_{\mathrm{MTS}}$, respectively. The dielectric superlayer is characterized by a dielectric constant ϵ_r and thickness h_s. The MTS will be made of metal strips of width w and periodicity d (fixed to $\lambda_0/4$ in this paper) for simplicity in their analysis since there is an analytical closed form expression for their reactance [25], [26]. This also means that the main parameter determining the properties of these LWAs is the complex transverse propagation constant k_ρ, of the TE_1 and TM_1 modes. Considering LWAs designed for broadside directivity enhancement, a smaller propagation constant (real and imaginary parts) implies higher directivity, but also smaller bandwidth and higher mutual coupling between two closed antennas placed under the same partially reflecting surface. The maximum power density at broadside for a small propagation constant occurs when $\alpha = \beta$ [23]. Therefore, when comparing different LWA configurations, an equivalence should be set by equalizing the corresponding $\mathrm{TE}_1/\mathrm{TM}_1$ propagation constants.

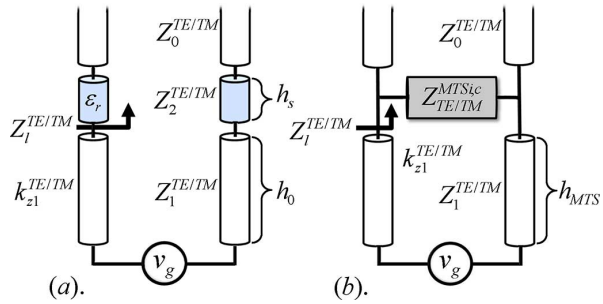

Fig. 2. Equivalent transmission line for (a) dielectric super-layer and (b) equivalent MTS.

A. Equivalent $\mathrm{TE}_1/\mathrm{TM}_1$ Modes

The leaky wave propagation constants are the solutions of the dispersion equation associated with the equivalent TE and TM transmission lines [9]. For the geometries under investigation here, the equivalent transmission lines are shown in Fig. 2. When the periodicity of the MTS is small compared to the wavelength, their electromagnetic properties can be represented by a purely imaginary shunt impedance $\mathrm{Z}_{\mathrm{TE/TM}}^{\mathrm{MTS}}$ [27]. We report the closed form expression for the impedances of the capacitive slot grid and inductive strip grid based MTS [25] since it would be necessary to derive analytical solutions of the dispersion equation:

$$Z_{\mathrm{TM}}^{\mathrm{MTSi}} = jX_0\left(1 - k_\rho^2/k_0^2\right) \tag{1}$$

$$Z_{\mathrm{TE}}^{\mathrm{MTSi}} = jX_0 \tag{2}$$

$$Z_{\mathrm{TM}}^{\mathrm{MTSc}} = -jX_0 \tag{3}$$

$$Z_{\mathrm{TE}}^{\mathrm{MTSc}} = -jX_0\left(1 - k_\rho^2/k_0^2\right)^{-1}. \tag{4}$$

where $X_0 = \eta_0 k_0 d/(2\pi)\ln|2d/(\pi w)|$ for $d \leq \lambda_0/4$ and η_0 is the free space wave impedance.

The dispersion equation associated to these equivalent transmission lines is the following:

$$D^{\mathrm{TE/TM}}(k_p) = Z_l + jZ_1 tan(k_{z1}h_1) = 0 \tag{5}$$

where $Z_l = Z_2(Z_0+jZ_2tan(k_{z2}h_2))/(Z_2+jZ_0tan(k_{z2}h_2))$ for the dielectric case and $Z_l = (Z^{i,c}_{\rm MTS}Z_0)/(Z^{i,c}_{\rm MTS}+Z_0)$ for the MTS. Z_0, Z_i represent the TE or TM impedances ($Z_i^{\rm TE} = \eta_0 k_0/k_{zi}$ and $Z_i^{\rm TM} = \eta_0 k_{zi}/k_0$), $h_1 = h_0$ or $h^{i,c}_{\rm MTS}$ and $k_{zi} = \sqrt{\epsilon_{ri}k_0^2 - k_\rho^2}$.

Therefore, the leaky wave propagation constant greatly depends on the load impedance, Z_l at the top of the cavity as shown in Fig. 2. The dispersion equation, once the geometry is known, can be solved numerically to find the leaky wave propagation constants. However, for design purposes, it is more convenient to have analytical approximate formulas to compute these constants. These formulas can be used to impose that equivalent LWAs have the $\rm TE_1/TM_1$ with the same propagation constants as proposed in [28], as well as to demonstrate that only the inductive strip grid based MTSs do not support the $\rm TM_0$ leaky mode, independently of the geometrical parameters. In [9], a methodology to derive these formulas for the $\rm TE_1/TM_1$ modes was proposed for dielectric based LWA and extended in [28] to MTS based LWA. The fundamental step was recognizing that the tangent function $\tan(x)$ can be linearly approximated around its zeroes for arguments in the neighborhood of $x \pm \pi$. Using this approximation the dispersion equation will be:

$$k_{z1} = j\frac{Z_l}{hZ_1} + \frac{n\pi}{h}. \tag{6}$$

Note that when the cavity load impedance Z_l will be equal to zero, this equation will give the propagation constants of the modes in a parallel plate waveguide (PPW) of thickness h. In order to make this equation analytical for the $n = 1$ in the TE and TM modes, the load impedance Z_l can be approximated by its value around broadside, therefore $Z_l = \eta_0/\epsilon_r$ for the dielectric superstrate or $Z_l = \eta_0 Z^{i,c}_{\rm MTS}(\theta = 0)/(\eta_0 + Z^{i,c}_{\rm MTS}(\theta = 0))$ for the MTS. By substituting these approximations into (6), one arrives to compact formulas for the $\rm TE_1/TM_1$ modes of LWAs [9], [28]. Then by equalizing both real and imaginary parts of the propagation constants, one can derive expressions for the MTS impedance and cavity height as a function of the parameters of the equivalent dielectric based LWA [28]. The expressions are reported here for convenience:

$$Z^{i,c}_{\rm MTS} = j\eta_0\left(\frac{-1 \pm \sqrt{1+4\pi^2(\epsilon_r-1)}}{2\pi(\epsilon_r-1)}\right) \tag{7}$$

$$h^{i,c}_{\rm MTS} = h_0\frac{\epsilon_r\left|Z^{i,c}_{\rm MTS}\right|^2}{\eta_0^2 + \left|Z^{i,c}_{\rm MTS}\right|^2}. \tag{8}$$

Figs. 3 and 4 show the $\rm TE_1$ and $\rm TM_1$ dispersion diagrams for the three equivalent geometries under investigation, i.e., dielectric superstrate (blue line), inductive strip grid based MTS (red line) and capacitive slot grid based MTS (black line). All curves are calculated for equivalent superstrate permittivity $\epsilon_r = 4$ (continuous line) and $\epsilon_r = 10$ (dashed line). The equivalent inductive strip grid based MTS has $Z^i_{\rm MTS} = 119i\Omega$ and must be located at a height of $h^i_{\rm MTS} = 0.9h_0$ whilst the capacitive slot grid based MTS has $Z^c_{\rm MTS} = -132i\Omega$ and needs to be placed at a height of $h^c_{\rm MTS} = 1.10\,h_0$ for $\epsilon_r = 10$ whilst $Z^i_{\rm MTS} = 199i\Omega$, $h^i_{\rm MTS} = 0.87h_0$, $Z^c_{\rm MTS} = -238i\Omega$ and $h^c_{\rm MTS} = 1.14\,h_0$ for

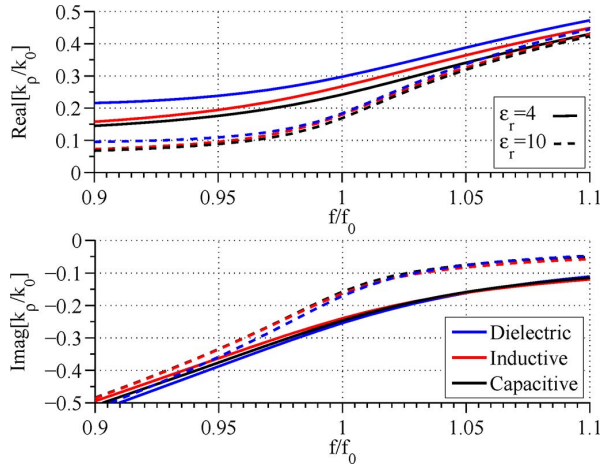

Fig. 3. $\rm TE_1$ mode solution of the dispersion equation with $\epsilon_r = 4$ (continuous lines) and $\epsilon_r = 10$ (dashed lines) for three equivalent cases: dielectric superstrate (blue), inductive strip grid based MTS (red) and capacitive slot grid based MTS (black).

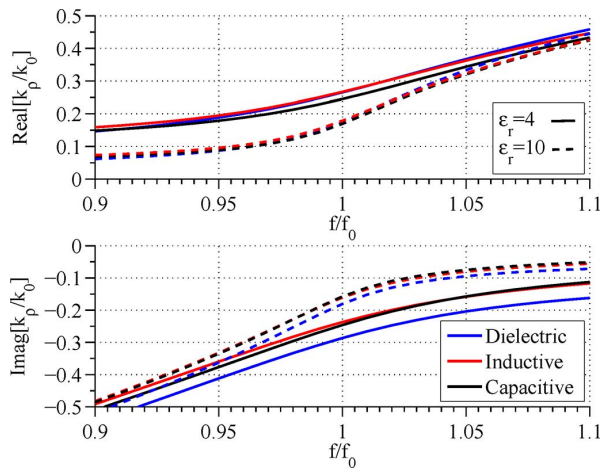

Fig. 4. $\rm TM_1$ mode solution of the dispersion equation with $\epsilon_r = 4$ (continuous lines) and $\epsilon_r = 10$ (dashed lines) for three equivalent cases: dielectric superstrate (blue), inductive strip grid based MTS (red) and capacitive slot grid based MTS (black).

TABLE I
COMPARISON OF THE PROPAGATION CONSTANTS OBTAINED FOR THE EQUIVALENT MTSS AND $\epsilon_r = 10$ DIELECTRIC LWAS AT CENTRAL FREQUENCY

k_ρ/k_0	Dielectric	Inductive	Capacitive
TE	$0.184 - j0.171$	$0.179 - j0.163$	$0.169 - j0.158$
TM	$0.174 - j0.181$	$0.179 - j0.161$	$0.169 - j0.158$
TM_0	$0.972 - j0.034$	$1 - j0$	$0.979 - j0.029$
h_{MTS}	h_0	$0.9h_0$	$1.1h_0$

$\epsilon_r = 4$, being $h_0 = \lambda_0/2$. It can be observed that the equivalent geometries present comparable solutions of the dispersion equation around the operating frequency ($\rm f/f_0 = 1$) at which maximum broadside radiation occurs. A larger discrepancy is observed for lower dielectric constants since the approximate analytical formulas lose accuracy for lower contrast as pointed out in [9]. Table I gives the numerical solutions of the dispersion equation of the three equivalent LWAs for $\epsilon_r = 10$ at the central frequency.

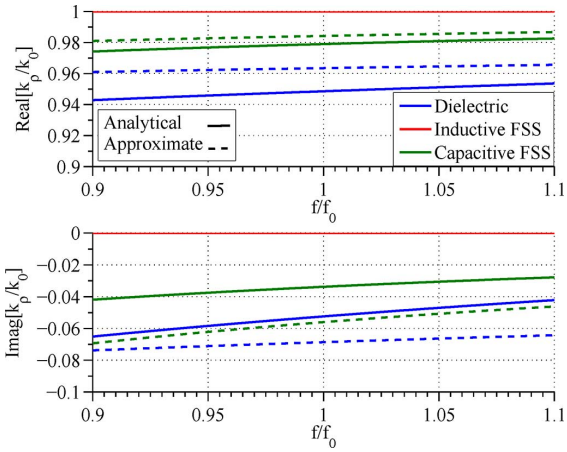

Fig. 5. TM_0 mode of the numerical (continuous lines) and approximate (dashed lines) solution of the dispersion equation with $\epsilon_r = 4$ for three equivalent cases: dielectric superstrate (blue), inductive strip grid based MTS (red) and capacitive slot grid based MTS (green).

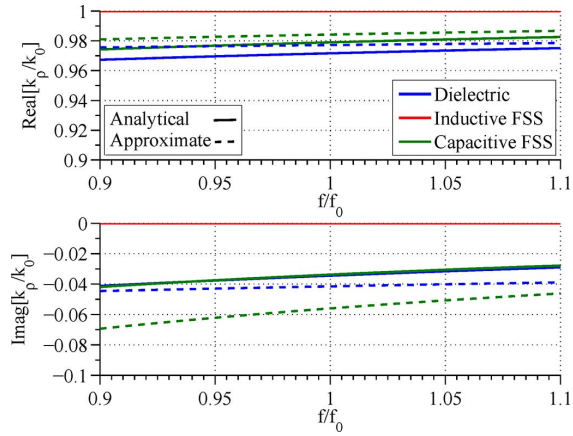

Fig. 6. TM_0 mode of the numerical (continuous lines) and approximate (dashed lines) solution of the dispersion equation with $\epsilon_r = 10$ for three equivalent cases: dielectric superstrate (blue), inductive strip grid based MTS (red) and capacitive slot grid based MTS (green).

B. *Analytical Dispersion Equation Solution for the* TM_0 *Mode*

Following similar steps, a formula can also be obtained for the $\mathrm{n} = 0$ TM mode. In this case, the TM dispersion equation becomes:

$$Z_l + j\frac{\eta_0 k_{z1}^2}{h_1 k_0} = 0. \tag{9}$$

In a PPW, the TEM mode has the electric field oriented along z and therefore its transverse propagation constant is $k_\rho \approx k_0$. To derive an analytical formula for the leaky wave TM_0 mode, we can approximate the load impedance Z_l by its value around $k_\rho \approx k_0$. The steps for this derivation are summarized in Appendix I for the cases shown in Fig. 1. The final formulas are reported here:

$$k_{z1}^{\mathrm{SUP}} = \sqrt[3]{jk_0^2\frac{\epsilon_r - 1}{\epsilon_r^2 h_0}} \tag{10}$$

$$k_{z1}^{\mathrm{IND}} = 0 \tag{11}$$

$$k_{z1}^{\mathrm{CAP}} = -j\frac{X_0 k_0}{2\eta_0}\left(1 + \sqrt{1 + \frac{4\eta_0}{k_0 X_0 h_{\mathrm{MTS}}}}\right). \tag{12}$$

The associated transverse propagation constant can be easily calculated by using $k_\rho = \sqrt{k_0^2 - k_{z1}^2}$.

From these equations, we can see that the inductive strip grid based MTS is the only configuration which does not support a TM_0 leaky wave, independently of the MTS geometrical parameters. This is because, the TM_0 mode is mainly z-polarized and the strips are nearly transparent for this polarization. The TM_0 mode in this inductive MTS is transformed into a surface wave (SW) that will only alter the radiation pattern by diffraction at the edges of the structure. The impact on the radiation pattern of both a TM_0 leaky mode and a surface wave can be reduced by introducing a spectral null at $k_\rho = k_\rho^{\mathrm{TM}_0}$ [19], [21]. However, as it will be shown in Section III, the inductive MTS still leads to the highest directivity enhancement. We will see next how this implies that the radiated field generated by the inductive strip grid based MTS has a larger roll-off than the one radiated by the dielectric and capacitive based LWAs.

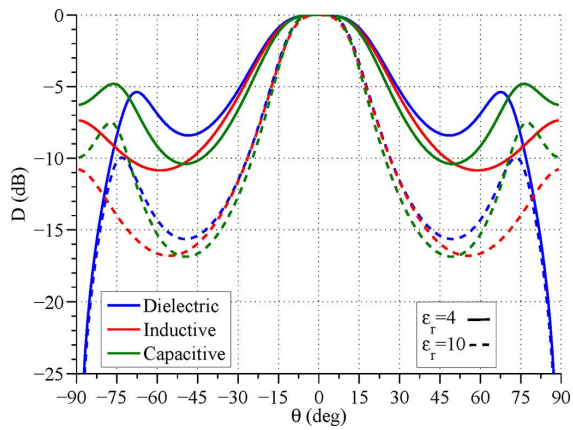

Fig. 7. $E-plane$ Comparison of theoretical radiation patterns for the equivalent structures described in Fig. 1 at $f = f_0$.

Figs. 5 and 6 show the exact and approximate solutions of the dispersion equation for the TM_0 mode for the same cases than in Figs. 3 and 4. Once again, the accuracy of the analytical formulas is higher for higher contrast since the solution get closer to the PPW ones. The exact solution for the TM_0 mode is also given in Table I.

C. *Theoretical Far-Fields*

Next we investigate the radiated fields in the far-field by the three equivalent LWAs. These patterns can be obtained resorting to a rigorous spectral Green's function approach [24]. Figs. 7 and 8 show the radiated fields for an elementary source at central frequency in E- and H-plane, respectively, for the same structures described in Figs. 3 and 4. An important consequence of the TM_0 suppression is observed in the E-plane. In fact, for the dielectric case the existence of the TM_0 mode causes a side lobe in an angular direction close to the Brewster angle. For the capacitive slot grid based MTS, the effect of the TM_0 is also observed, but at a slightly larger angle. For inductive strip grid based MTS, this peak disappears, with the consequent increase of directivity.

Fig. 9 shows the estimated directivity as a function of the frequency for the three equivalent LWAs for the denser contrast

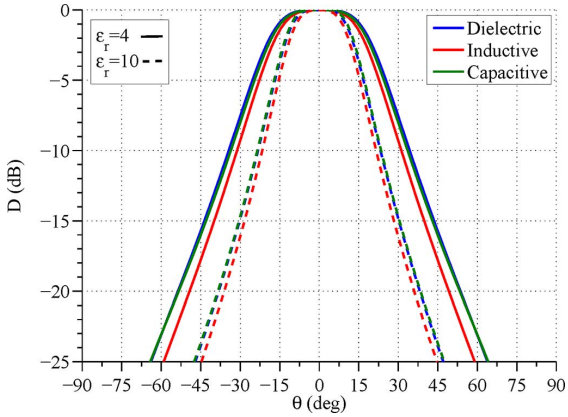

Fig. 8. $H-plane$ Comparison of theoretical radiation patterns for the equivalent structures described in Fig. 1 at $f = f_0$.

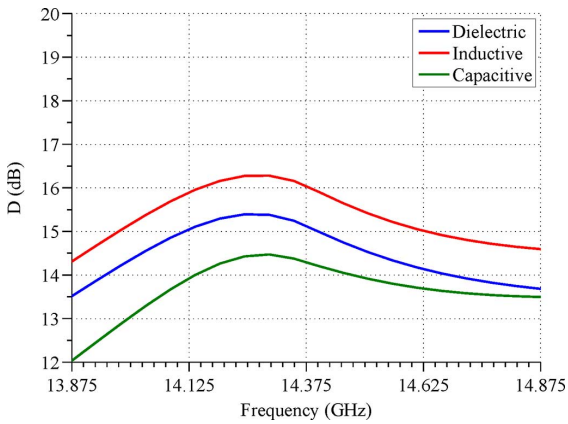

Fig. 9. Directivity as a function of the frequency for the equivalent LWA starting from $\epsilon_r = 10$. The dielectric LWA bandwidth is BW $= 3.8\%$, whilst the bandwidth for the inductive and capacitive-based LWAs is 3.7% and BW $= 5.7\%$, respectively.

case of Figs. 7 and 8. As it can be appreciated, the inductive solution improves the directivity in almost 1 dB over the frequency band with respect to the dielectric solution. It is also important to notice that the calculated frequency bandwidth of the LWAs, defined here as when the directivity decays 1 dB from the maximum, is the same for the three structures (the precise values are given in the figure caption).

III. LWA Designs For Array Applications

In this section, we present three antenna designs based on the geometries shown in Fig. 1 that could be used for the application scenario described in the introduction. The three equivalent solutions take as baseline a dielectric constant $\epsilon_r = 10$ and fulfill the equivalence condition derived previously. In contrast with the previous section, here the structures have been analyzed using a commercial software [29] including a waveguide source and a finite ground plane/superstrate ($9.9\lambda_0$ by side). The effect of the TM_0 can be reduced by using a double slot opening in a ground plane as proposed in [19], (see Fig. 10). In the inductive strip grid based MTS case the double slot iris is used to avoid the power loss related to the SW. Therefore it is important to understand if the directivity increase for the inductive strip grid based MTS is still achieved with respect to a well-designed dielectric

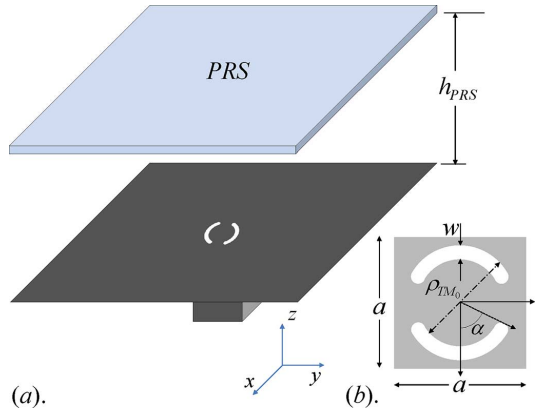

Fig. 10. Description of the basic antenna and iris used to feed the cavity. The parameters of the slots in the iris are $a = 14.6$ mm, $w = 0.5$ mm, $\rho_{\mathrm{TM}_0} = 10.79$ mm and $\alpha = 79$ deg. The squared waveguide has a length of $wg = 0.7\lambda_0$ by side.

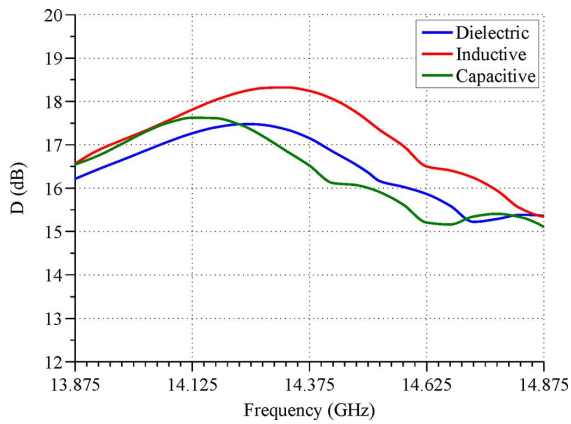

Fig. 11. Directivity as a function of the frequency for the equivalent structures described in Fig. 1. The waveguide dimension is $w_g = 0.7\lambda_0$ and the width of the iris has been fixed to w $= 0.51$ mm whilst the diameter of the iris has been fixed to $\lambda_{TM_0}/2$ of each case (10.73 mm, 10.43 mm and 10.66 mm for dielectric, inductive strip grid and capacitive slot grid based MTS respectively). The 1 dB directivity BW is 3.86% for dielectric, 3.51% for the inductive and 3.3% for the capacitive case respectively.

TABLE II
Directivities for the Equivalent MTS and Dielectric Geometries With $\epsilon_r = 10$ at Central Frequency and Maximum Value in the Band

Directivity (dB)	Dielectric	Inductive	Capacitive
ϵ_r=10 at f_0	17.1	18.24	16.52
ϵ_r=10 at best performance	17.48	18.32	17.62

based LWA. This iris can also be used to match the reflection coefficient S_{11} of the antenna.

Fig. 11 presents simulated directivities versus the frequency. All the cases present higher directivities with respect to the theoretical results of Fig. 9 due to the inclusion of an actual source feeding the LW cavity. The capacitive case presents also a small frequency shift. Even with the inclusion of the source and suppression of the TM_0 mode, the inductive LWA presents higher directivities over comparable bands. The values of the maximum directivities for each case are summarized in Table II for the central frequency $f_0 = 14.375$ GHz. The radiation patterns for each design are shown in Figs. 12 and 13 for the E- and

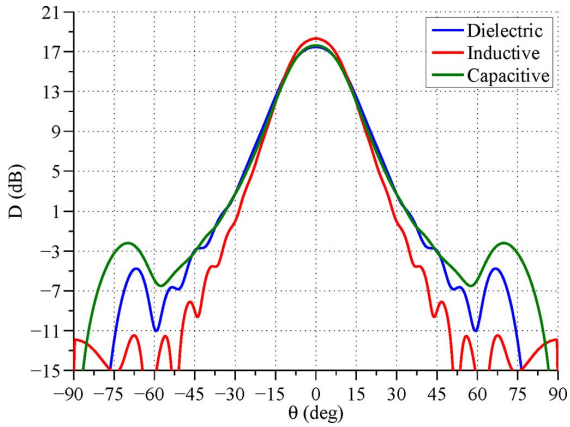

Fig. 12. $E-plane$ Comparison of CST simulated radiation patterns for the equivalent structures described in Fig. 11 at the frequency with highest directivity.

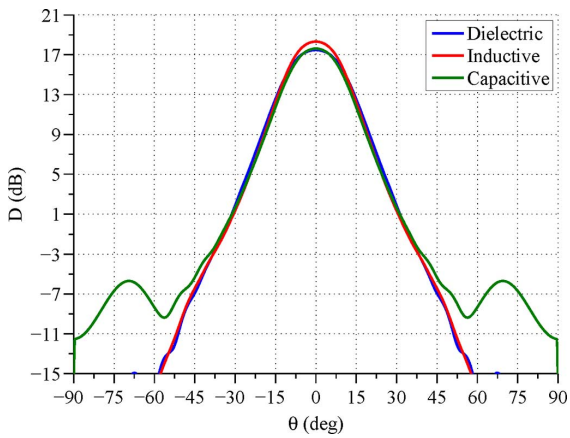

Fig. 13. $H-plane$ Comparison of CST simulated radiation patterns for the equivalent structures described in Fig. 11 at the frequency with highest directivity.

H-plane, respectively, at the frequency at which the directivity is the highest.

IV. Experimental Verification

In order to validate the claim of the paper, we have fabricated and measured two prototypes: the dielectric and the inductive based LWA. The dielectric material used for the super-layer is AR1000 with permittivity $\epsilon_r = 10$ and a thickness of 1.57 mm. The operation frequency is set to 14.375 GHz. Fig. 14 shows the designed transition, together with the geometrical parameters, from a squared waveguide to a standard rectangular waveguide, necessary for measuring the manufactured prototype. Both manufactured LWA will use the same waveguide feed for simplicity. The MTS has been printed on a Kapton layer (with 0.05 mm thickness and $\epsilon_r = 3$). This is a flexible material that has been supported by a thin foam layer (with 3 mm thickness and $\epsilon_r = 1.067$) for the prototype. The inclusion of these layers alters the leaky wave propagation constants for the MTS case. This change can be easily compensated by modifying the cavity dimensions and strip dimensions. To this purpose, we have calculated the solution of the dispersion equation associated with the transmission line model shown in Fig. 15. The new cavity

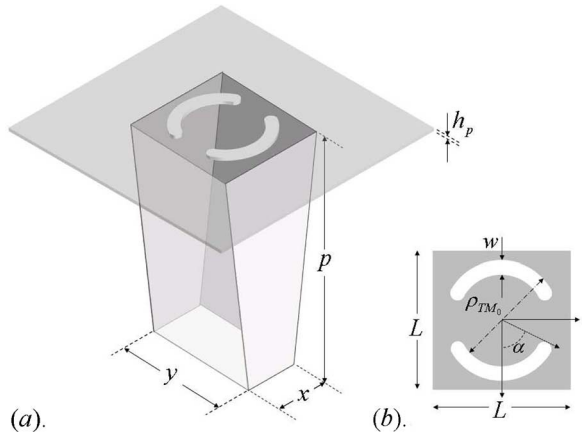

Fig. 14. Description of the iris and transition used to feed the cavity. The parameters of the feeder are for the transition $x = 6.48$ mm, $y = 12.95$ mm, $p = 45.22$ mm, $h_p = 0.5$ mm and the slots in the iris $L = 14.6$ mm, $w = 0.5$ mm, $\rho_{\mathrm{TM}_0} = 10.79$ mm, $\alpha = 79$ deg. The same basic antenna will be used in both dielectric and inductive strip grid based MTS.

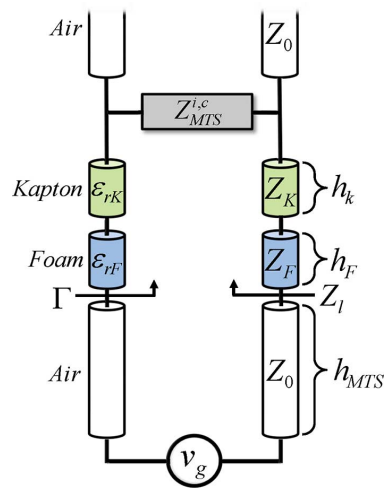

Fig. 15. Practical realization of the inductive strip grid based MTS LWA.

TABLE III
Original and Optimized Inductive Strip Grid Based MTS Design

Inductive strip grid based MTS	k_{z1}^{TE}	k_{z1}^{TM}
air	$0.179 - 0.163i$	$0.179 - 0.161i$
Kapton+foam (no optimized)	$0.156 - 0.163i$	$0.156 - 0.163i$
Kapton+foam (optimized)	$0.179 - 0.163i$	$0.179 - 0.161i$

dimension is $\mathrm{h_{MTS}} = 6.41$ mm and the width of the strip w has changed from the original value of 0.94 mm to 1 mm. By changing these parameters, we have been able to obtain the same leaky wave propagation constant as the free standing MTS based LWA, as it is detailed in Table III.

The simulated radiation patterns of the two prototypes are presented in Fig. 16. The total antenna size is $9.91 \times 9.91\lambda_0$. We have also included the losses (i.e., for the foam is $\tan\delta = 0.0041$) and thickness of metals in the simulations. From the simulations a clear increase in directivity is observed for the inductive strip grid based MTS based LWA. This increase is approximately 1.6 dB. The simulated directivity in the frequency band is shown in Fig. 17.

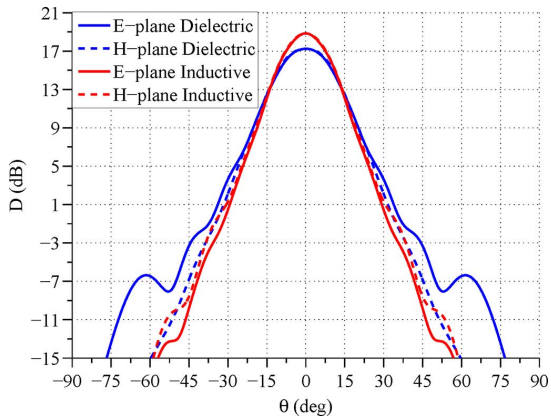

Fig. 16. Simulated radiation pattern for the two prototypes. The directivity of the dielectric super-layer and inductive strip grid based MTS antenna are 17.2 dB and 18.8 dB respectively at f = 14.25 GHz. Both antennas are fed with the iris shown in Fig. 14.

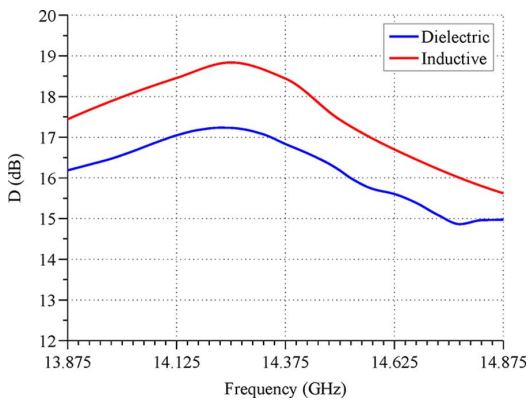

Fig. 17. Simulated directivity in dB for the dielectric and equivalent inductive antennas. The BW is respectively 4.23% and 3.45% for the dielectric and MTS prototype with iris and transition.

A. Study of the Fabrication Tolerances

Before starting the fabrication of the prototypes, a complete analysis of the fabrication tolerances was carried out. The most critical parameters are associated with the highly resonant cavity. The first critical parameter is the height of the cavity h_{MTS}. The impact of the height of the cavity over the radiated fields was already reported in [30]. A variation in our design of around $h_{MTS} + 10\%$ (i.e., in the inductive strip grid based MTS LWA) decreases the directivity around 2 dB and moves the resonance at lower frequencies whilst a small variation of $h_{MTS} - 10\%$ decreases the directivity around 1 dB and moves the resonance at higher frequencies. It is worth noting that this parameter has also an important impact on the reflection coefficient. The second parameter that has been studied is a tilt angle of the MTS layer. We have done several simulations of the MTS antenna varying this angle. This parameter affects more strongly the radiation pattern than the matching of the reflection coefficient compared to the other parameters. The effect of this parameter over the radiation pattern is a loss of directivity and a deviation of the pointing angle as this alters the phase distribution over the antenna aperture. A small deviation of 0.3 deg in this design of $9.91 \times 9.91\lambda_0$ represents a loss

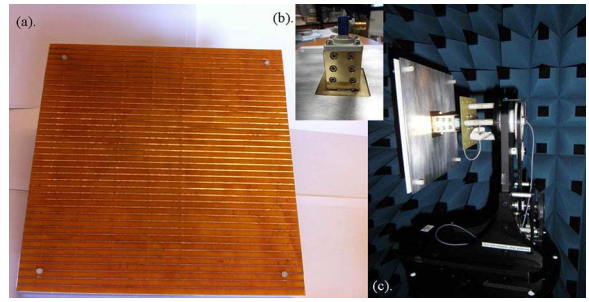

Fig. 18. Prototype photos for (a). MTS (b). Waveguide transition (c). Measurement set-up.

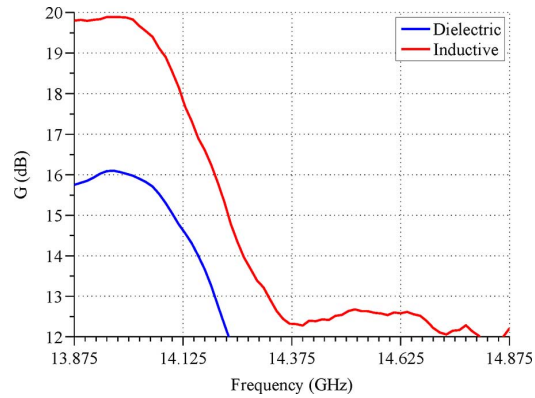

Fig. 19. Measured gain for the dielectric and equivalent inductive LWAs. The BW is 2.52% for both prototypes.

of directivity of around 1 dB and a misalignment of the main lobe of around 5 deg. Taking into account these considerations, we have built and measured the prototype to the best of our laboratory facilities.

B. Measurements

The fabricated prototypes are shown in Fig. 18. Fig. 19 shows the measured gain as a function of the frequency. A frequency shift with respect to the simulated directivity shown in Fig. 17 has been measured for both the dielectric and inductive based LWAs. The height of the cavity is a sensitive parameter in this type of antennas, and it has to be manually adjusted during the measurements. A more accurate fabrication process would resolve this shift. Despite that, the dielectric and inductive measured gain presents same BW of around 2.52%. The maximum gain is measured at f = 13.9 GHz. At this frequency the dielectric super-layer and inductive strip grid based MTS antenna have 16.6 dB and 19.6 dB of directivity respectively (see Fig. 20).

Fig. 20 shows the measured radiation patterns for the two prototypes in the main planes at f = 13.9 GHz. It is evident that the measured radiation patterns agree quite well with the simulated ones, despite the measured frequency shift.

The measured S_{11} is shown in Fig. 21 for both, dielectric and inductive strip grid based MTS cases. In the same graph, the results from full wave simulations are included for comparison purposes. Both antennas present comparable frequency bandwidths. The agreement is quite satisfactory and no significant frequency shift is observed in this case. The measurement

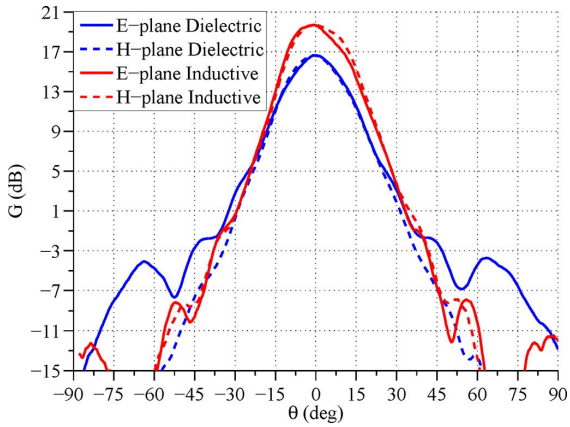

Fig. 20. Measured radiation pattern for the two prototypes. The measured gain of the dielectric super-layer and inductive strip grid based MTS antennas are 16.6 dB and 19.6 dB respectively at f = 13.9 GHz. Both antennas are fed with the iris shown in Fig. 14.

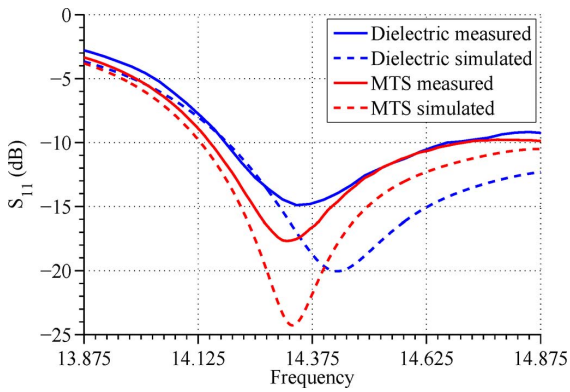

Fig. 21. Measured S_{11} for the dielectric and equivalent inductive antennas. Simulated results are also included for comparison purposes. The BW of the reflection coefficients S_{11} are 3.62% and 3.90% for the measured dielectric and MTS prototypes respectively.

campaign for the Fig. 21 has been done at a different measurement facility. We believe that the cavity height was not placed at exactly the same position than in the radiation pattern measurements.

V. Conclusion

In this work, we have rigorously compared the performances of LWAs based on dielectric superlayers with LWAs based on inductive strip and capacitive slot grid based MTS by imposing an equivalence in terms of the fundamental TE/TM modes. This equivalence ensures that the three antennas have comparable frequency bandwidths and levels of mutual coupling if they were to be used in array configurations. We have found that the inductive strip grid based MTS leads to the highest directivity enhancement for the same bandwidth. The radiation patterns have a higher roll-off of the radiation pattern by cause of the symmetrical leaky wave TE_1/TM_1 modes and the suppression of a spurious large angle TM_0 leaky-wave mode. The suppression of this mode is demonstrated rigorously with simple and controllable closed form formulas.

Numerical full wave analysis and experiments have confirmed the theory showing an improved directivity of more than 1 dB with the same frequency band of operation. This improvement is especially significant for thinned phased arrays and focal plane arrays based on LWA elements.

Appendix A
Approximate Formulas To Compute the TM_0 Mode

In this Appendix, we present the methodology to derive an approximate analytical formula for calculating the TM_0 propagation constant. The dispersion equation that we would like to solve is the one given in (5) for the three configurations shown in Fig. 1. Approximating the tan function around its n = 0 zero, one arrives to the following dispersion equation:

$$Z_l + j\frac{\eta_0 k_{z_1}^2}{h_1 k_0} = 0. \tag{13}$$

In order to derive an analytical solution, we need to provide an approximate but accurate expression for the load impedance Z_l. We can do this by recalling that the modes in a LWA resemble those of the equivalent PPW. In a PPW, the TEM mode transverse propagation constant is $k_\rho = k_0$. Therefore, when looking for the solution of the TM_0 mode, we can approximate Z_l by its value around $k_\rho = k_0$. This is done in the following for three specific cases shown in Fig. 1.

A. Dielectric Superstrate

In this case, the load impedance Z_l is given by $Z_l = Z_2(z_0 + jz_2\tan(k_{z2}h_2))/(z_2 + jz_0 tan(k_{z2}h_2))$.

For $k_\rho = k_0$, the dielectric characteristic TM impedance becomes $z = \eta_0\sqrt{(\epsilon_r - 1)}/\epsilon_r$ and $Z_l \approx z_2^2/z_0$.

Substituting these approximations into (13), one arrives to the following formula of the longitudinal propagation constant for the TM_0 mode:

$$k_{z1}^{\mathrm{SUP}} = \sqrt[3]{jk_0^2\frac{\epsilon_r - 1}{\epsilon_r^2 h_0}}. \tag{14}$$

B. LWA Based MTS

For the MTS cases, the load impedance is calculated by $Z_l = (Z_{\mathrm{MTS}}^{i,c} Z_0)/(Z_{\mathrm{MTS}}^{i,c} + Z_0)$.

Substituting this expression in (13), leads to

$$\frac{Z_{\mathrm{TM}}^{\mathrm{MTS}}\eta_0 k_{z1}}{k_0} + j\frac{\eta_0 h_1 k_{z1}^2}{k_0}\left(Z_{\mathrm{TM}}^{\mathrm{MTS}} + \frac{\eta_0 k_{z1}}{z_0}\right) = 0. \tag{15}$$

Thus one solution is $k_{z1} = 0$, and other two solutions come from the following equation

$$Z_{\mathrm{TM}}^{\mathrm{MTS}} + jh_1 k_{z1} Z_{\mathrm{TM}}^{\mathrm{MTS}} + jh_1\eta_0\frac{k_{z1}^2}{z_0} = 0. \tag{16}$$

For inductive strip grid based MTS, the impedance is given by (1), which in the E-plane can be written as

$$Z_{\mathrm{TM}}^{\mathrm{MTSi}} = j\frac{X_0 k_{z1}^2}{k_0^2}. \tag{17}$$

This expression can be replaced in (16), giving rise to two solutions: again $k_{z1}^{\mathrm{IND}} = 0$ and $k_{z1}^{\mathrm{IND}} = j(h_1\eta_0 k_0 + X_0)/(X_0 h_1)$. This second solution is non-physical. Therefore the only

possible solution for the inductive strip grid based MTS is $k_{z1}^{\mathrm{IND}} = 0$.

In the capacitive slot grid based MTS case, the impedance in the E plane is the following

$$Z_{\mathrm{TM}}^{\mathrm{MTSc}} = -jX_0. \tag{18}$$

Replacing this expression into (16), one arrives to the following physical solution:

$$k_{z1}^{\mathrm{CAP}} = -j\frac{X_0 k_0}{2\eta_0}\left(1+\sqrt{1+\frac{4\eta_0}{X_0 h_1 k_0}}\right). \tag{19}$$

ACKNOWLEDGMENT

The authors would like to express their gratitude to Dr. Masa-Campos and P. Sánchez-Olivares from the Autonomous University of Madrid for their help in the antenna measurement process. They would also like to thank EADS/CASA for providing the Ku-band array specifications.

REFERENCES

[1] G. Trentini, "Partially reflecting sheet arrays," *IEEE Trans. Antennas Propag.*, vol. 4, no. 4, pp. 666–671, Oct. 1956.

[2] D. Jackson, A. Oliner, and A. Ip, "Leaky-wave propagation and radiation for a narrow-beam multiple-layer dielectric structure," *IEEE Trans. Antennas Propag.*, vol. 41, no. 3, pp. 344–348, Mar. 1993.

[3] C. Cheype, C. Serier, M. Thevenot, T. Monediere, A. Reineix, and B. Jecko, "An electromagnetic bandgap resonator antenna," *IEEE Trans. Antennas Propag.*, vol. 50, no. 9, pp. 1285–1290, Sep. 2002.

[4] T. Zhao, D. Jackson, J. Williams, H. Yang, and A. Oliner, "2-D periodic leaky-wave antennas–Part I: Metal patch design," *IEEE Trans. Antennas Propag.*, vol. 53, no. 11, pp. 3505–3514, Nov. 2005.

[5] T. Zhao, D. Jackson, and J. Williams, "2-D periodic leaky-wave antennas-part II: Slot design," *IEEE Trans. Antennas Propag.*, vol. 53, no. 11, pp. 3515–3524, Nov. 2005.

[6] A. Feresidis, G. Goussetis, W. Shenhong, and J. Vardaxoglou, "Artificial magnetic conductor surfaces and their application to low-profile high gain planar antennas," *IEEE Trans. Antennas Propag.*, vol. 53, no. 1, pp. 209–215, Jan. 2005.

[7] Y. Lee, Y. J., R. Mittra, and W. Park, "Application of electromagnetic bandgap (EBG) superstrates with controllable defects for a class of patch antennas as spatial angular filters," *IEEE Trans. Antennas Propag.*, vol. 53, no. 1, pp. 224–235, Jan. 2005.

[8] N. Guerin, S. Enoch, G. Tayeb, P. Sabouroux, P. Vincent, and H. Legay, "A metallic fabry-perot directive antenna," *IEEE Trans. Antennas Propag.*, vol. 54, no. 1, pp. 220–224, Jan. 2006.

[9] A. Neto and N. Llombart, "Wideband localization of the dominant leaky wave poles in dielectric covered antennas," *IEEE Antennas Wireless Propag. Lett.*, vol. 5, no. 1, pp. 549–551, Dec. 2006.

[10] G. Lovat, P. Burghignoli, and D. Jackson, "Fundamental properties and optimization of broadside radiation from uniform leaky-wave antennas," *IEEE Trans. Antennas Propag.*, vol. 54, no. 5, pp. 1442–1452, May 2006.

[11] A. Foroozesh and L. Shafai, "Investigation into the effects of the patch-type FSS superstrate on the high-gain cavity resonance antenna design," *IEEE Trans. Antennas Propag.*, vol. 58, no. 2, pp. 258–270, Feb. 2010.

[12] M. Pasian, M. Bozzi, and L. Perregrini, "Design of a large bandwidth planar antenna using inductive frequency selective surfaces," in *Proc. 2nd Eur. Conf. on Antennas and Propagation, EuCAP*, Nov. 2007, pp. 1–5.

[13] K. Sarabandi and N. Behdad, "A frequency selective surface with miniaturized elements," *IEEE Trans. Antennas Propag.*, vol. 55, no. 5, pp. 1239–1245, May 2007.

[14] P. Burghignoli, G. Lovat, F. Capolino, D. Jackson, and D. Wilton, "Highly polarized, directive radiation from a Fabry-Pérot cavity leaky-wave antenna based on a metal strip grating," *IEEE Trans. Antennas Propag.*, vol. 58, no. 12, pp. 3873–3883, Dec. 2010.

[15] N. Llombart, A. Neto, G. Gerini, M. Bonnedal, and P. de Maagt, "Leaky wave enhanced feed arrays for the improvement of the edge of coverage gain in multibeam reflector antennas," *IEEE Trans. Antennas Propag.*, vol. 56, no. 5, pp. 1280–1291, May 2008.

[16] C. Menudier, R. Chantalat, E. Arnaud, M. Thevenot, T. Monediere, and P. Dumon, "EBG focal feed improvements for Ka-band multibeam space applications," *IEEE Antennas Wireless Propag. Lett.*, vol. 8, pp. 611–615, 2009.

[17] R. Gardelli, M. Albani, and F. Capolino, "Array thinning by using antennas in a Fabry-Perot cavity for gain enhancement," *IEEE Trans. Antennas Propag.*, vol. 54, no. 7, pp. 1979–1990, Jul. 2006.

[18] D. Blanco, N. Llombart, and E. Rajo-Iglesias, "On the use of leaky wave phased arrays for the reduction of the grating lobe level," *IEEE Trans. Antennas Propag.*, vol. 62, no. 4, pp. 1789–1795, Apr. 2014.

[19] N. Llombart, A. Neto, G. Gerini, M. Bonnedal, and P. de Maagt, "Impact of mutual coupling in leaky wave enhanced imaging arrays," *IEEE Trans. Antennas Propag.*, vol. 56, no. 4, pp. 1201–1206, Apr. 2008.

[20] A. Polemi and S. Maci, "On the polarization properties of a dielectric leaky wave antenna," *IEEE Antennas Wireless Propag. Lett.*, vol. 5, no. 1, pp. 306–310, Dec. 2006.

[21] M. Qiu, G. Eleftheriades, and M. Hickey, "A reduced surface-wave twin arc-slot antenna element on electrically thick substrates," in *Proc. IEEE Antennas and Propagation Society Int. Symp.*, Jul. 2001, vol. 3, pp. 268–271, vol. 3.

[22] W. Syed and A. Neto, "Front-to-back ratio enhancement of planar printed antennas by means of artificial dielectric layers," *IEEE Trans. Antennas Propag.*, vol. 61, no. 11, pp. 5408–5416, Nov. 2013.

[23] D. Jackson, P. Burghignoli, G. Lovat, F. Capolino, J. Chen, D. Wilton, and A. Oliner, "The fundamental physics of directive beaming at microwave and optical frequencies and the role of leaky waves," *Proc. IEEE*, vol. 99, no. 10, pp. 1780–1805, Oct. 2011.

[24] A. Neto, N. Llombart, G. Gerini, D. Bonnedal, and P. de Maagt, "EBG enhanced feeds for the improvement of the aperture efficiency of reflector antennas," *IEEE Trans. Antennas Propag.*, vol. 55, no. 8, pp. 2185–2193, Aug. 2007.

[25] O. Luukkonen, C. Simovski, G. Granet, G. Goussetis, D. Lioubtchenko, A. Raisanen, and S. Tretyakov, "Simple and accurate analytical model of planar grids and high-impedance surfaces comprising metal strips or patches," *IEEE Trans. Antennas Propag.*, vol. 56, no. 6, pp. 1624–1632, Jun. 2008.

[26] N. Marcuvitz, "Waveguide Handbook," Volume 10 in the Massachusetts Institute of Technology Radiation Laboratory Series 1965.

[27] D. Sievenpiper, Z. Lijun, R. Broas, N. Alexopolous, and E. Yablonovitch, "High-impedance electromagnetic surfaces with a forbidden frequency band," *IEEE Trans. Microwave Theory Tech.*, vol. 47, no. 11, pp. 2059–2074, Nov. 1999.

[28] M. Etorre, "Analysis and Design of Efficient Planar Leaky-Wave Antennas," Ph.D. dissertation, University of Siena, Siena, Italy, 2008.

[29] Spatial corp, "CST Studio Suite," Sep. 29, 2012 [Online]. Available: http://www.cst.com, release version 2012.06

[30] A. Neto, M. Ettorre, G. Gerini, and P. de Maagt, "Leaky wave enhanced feeds for multibeam reflectors to be used for telecom satellite based links," *IEEE Trans. Antennas Propag.*, vol. 60, no. 1, pp. 110–120, Jan. 2012.

Darwin Blanco received the Electrical Engineering degree from the University of Antioquia, Colombia, in 2009, the M.Sc. and Ph.D. (*summa cum laude*) degrees in multimedia and communications from the University Carlos III de Madrid UC3M, Madrid, Spain, in 2011 and 2014, respectively.

His current research interests include leaky wave antennas, frequency selective surfaces and phase array antennas.

Eva Rajo-Iglesias (SM'12) was born in Monforte de Lemos, Spain, in 1972. She received the M.Sc. degree in telecommunication engineering from the University of Vigo, Spain, in 1996, and the Ph.D. degree in telecommunication engineering from the University Carlos III of Madrid, Spain, in 2002.

She was a Teacher Assistant with the University Carlos III of Madrid from 1997 to 2001. She joined the Polytechnic University of Cartagena, Cartagena, Spain, as a Teacher Assistant, in 2001. She joined University Carlos III of Madrid as a Visiting Lecturer in 2002, where she has been an Associate Professor with the Department of Signal Theory and Communications since 2004. She visited the Chalmers University of Technology, Gteborg, Sweden, as a Guest Researcher, in 2004, 2005, 2006, 2007, and 2008, and has been an Affiliate Professor with the Antenna Group, Signals and Systems Department, since 2009. She has coauthored more than 50 papers in JCR international journals and more than 100 papers in international conferences. Her current research interests include microstrip patch antennas and arrays, metamaterials, artificial surfaces and periodic structures, MIMO systems and optimization methods applied to electromagnetism.

Dr. Rajo-Iglesias was the recipient of the Loughborough Antennas and Propagation Conference Best Paper Award in 2007, the Best Poster Award in the field of Metamaterial Applications in Antennas, at the conference Metamaterials 2009, the 2014 Excellence Award to Young Research Staff at the University Carlos III of Madrid and the Third Place Winner of the Bell Labs Prize 2014. She is currently an Associate Editor of the *IEEE Antennas and Propagation Magazine* and of the *IEEE Antennas and Wireless Propagation Letters*.

Stefano Maci (F'14) is a Professor at the University of Siena (UNISI), Siena, Italy, and Director of the Ph.D. School of Information Engineering and Science, which presently includes about 60 Ph.D. students. Since 2000, he has been P.I. of ten research projects funded by the European Union (EU) and by the European Space Agency (ESA). In 2004, he founded the European School of Antennas (ESoA), a Ph.D. school that presently comprises 35 courses on antennas, propagation, and electromagnetic theory. He is the author of 130 papers published in international journals, 10 book chapters, and about 300 papers in proceedings of international conferences.

Prof. Maci is presently the Director of ESoA, a member of the Delegate Assembly of EurAAP (European Association of Antennas and Propagation), a member of the TAB (Technical Advisory Board) of the URSI Commission B, Chair of the Award Committee of the IEEE Antennas and Propagation Society (US), a member of the AP Executive Board of IET (UK), and a Distinguished Lecturer of the IEEE. He was the recipient of several awards, including the EurAAP Carrier Award in 2014.

Nuria Llombart (S'06–M'07–SM'13) received the Electrical Engineering and Ph.D. degrees from the Polytechnic University of Valencia, Spain, in 2002 and 2006, respectively.

During her Master's degree studies she spent one year at the Friedrich-Alexander University of Erlangen-Nuremberg, Germany, and worked at the Fraunhofer Institute for Integrated Circuits, Erlangen, Germany. From 2002 until 2007, she was with the Antenna Group, TNO Defence, Security and Safety Institute, The Hague, The Netherlands, working as a Ph.D. student and afterwards as a Researcher. From 2007 until 2010, she was a Postdoctoral Fellow at the California Institute of Technology, working for the Sub millimeter Wave Advance Technology Group, Jet Propulsion Laboratory, Pasadena, USA. She was a Ramón y Cajal Fellow at the Optics Department of the Complutense University of Madrid, Spain, from 2010 to 2012. In September 2012, she joined the THz Sensing Group at the Technical University of Delft, The Netherlands, where she is currently an Associate Professor. She has coauthored over 100 journal and international conference contributions. Her research interests include the analysis and design of planar antennas, periodic structures, reflector antennas, lens antennas, and waveguide structures, with emphasis in the THz range.

Dr. Llombart was co-recipient of the H.A. Wheeler Award for the Best Applications Paper of the year 2008 in the IEEE TRANSACTIONS ON ANTENNAS AND PROPAGATION, the 2014 THz Science and Technology Best Paper Award of the IEEE Microwave Theory and Techniques Society and several NASA awards. She also received the 2014 IEEE Antenna and Propagation Society Lot Shafai Mid-Career Distinguished Achievement Award. She serves as Topical Editor for the IEEE TRANSACTIONS ON THZ SCIENCE AND TECHNOLOGY, *IEEE Antennas and Propagation Wireless Letters*, and for the Antenna Applications Corner of the *IEEE Magazine on Antennas and Propagation*. She is also a Board Member of the IRMMW-THz International Society.